Soft Matter

Accepted Manuscript

ROYAL SOCIETY OF CHEMISTRY

www.rsc.org/softmatter

Table of contents

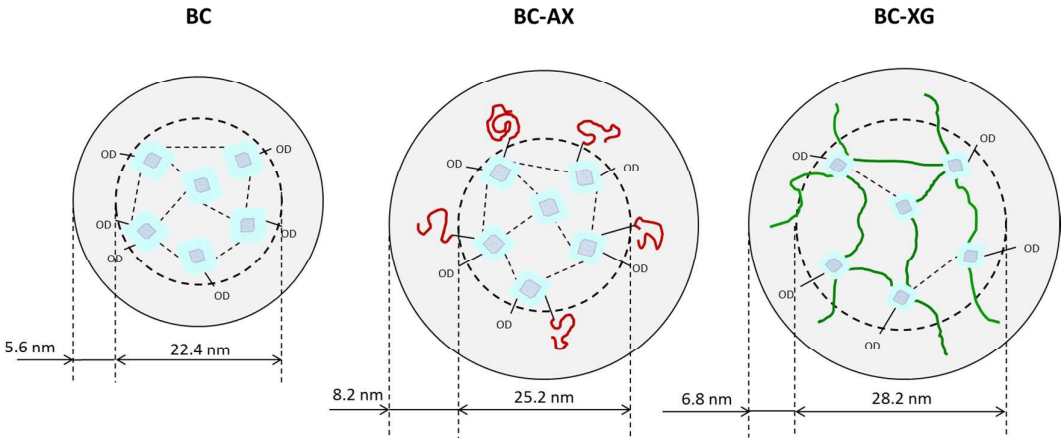

SANS data of bacterial cellulose and its composites with plant cell wall polysaccharides can be described by a core-shell model which accounts for the distinct solvent accessibility to the ribbons' inner/outer regions.

HIERARCHICAL ARCHITECTURE OF BACTERIAL CELLULOSE AND COMPOSITE PLANT CELL WALL POLYSACCHARIDE HYDROGELS USING SMALL ANGLE NEUTRON SCATTERING

Marta Martínez-Sanz [a,b], Michael J. Gidley [b] and Elliot P. Gilbert [a*]

[a] Bragg Institute, Australian Nuclear Science and Technology Organisation, Locked Bag 2001, Kirrawee DC, NSW 2232 (Australia).

[b] ARC Centre of Excellence in Plant Cell Walls, Centre for Nutrition and Food Sciences, University of Queensland, St. Lucia, Brisbane, QLD 4072 (Australia).

*Corresponding author: Tel.: +61 297179470; fax: +61 297173606

E-mail address: elliot.gilbert@ansto.gov.au

Abstract

Small angle neutron scattering (SANS) has been applied to characterise the structure of pure bacterial cellulose hydrogels, and composites thereof, with two plant cell wall polysaccharides (arabinoxylan and xyloglucan). Conventional published models, which assume that bacterial cellulose ribbons are solid one-phase systems, fail to adequately describe the SANS data of pure bacterial cellulose. Fitting of the neutron scattering profiles instead suggests that the sub-structure of cellulose microfibrils contained within the ribbons results in the creation of regions with distinct values of neutron scattering length density, when the hydrogels are subjected to H_2O/D_2O exchange. This may be represented within a core-shell formalism that considers the cellulose ribbons to comprise a core containing impermeable crystallites surrounded by a network of paracrystalline cellulose and tightly bound water, and a shell containing only paracrystalline cellulose and water. Accordingly, a fitting function comprising the sum of a power-law term to account for the large scale structure of intertwined ribbons, plus a core-shell cylinder with polydisperse radius, has been applied; it is demonstrated to simultaneously describe all SANS contrast variation data of pure and composite bacterial cellulose hydrogels. In addition, the resultant fitting parameters indicate distinct interaction mechanisms of arabinoxylan and xyloglucan with cellulose, revealing the potential of this approach to investigate the role of different plant cell wall polysaccharides on the biosynthesis process of cellulose.

Keywords: small angle scattering, neutron scattering, cellulose, hemicelluloses, bacterial cellulose

1. Introduction

Cellulose is one of the most abundant biopolymers found in nature, mostly as the main structural component of plant cell walls (PCWs). It is a linear homo-polysaccharide of β-D-glucopyranose linked by β-1-4-linkages which, in its native form, is found assembled in a characteristic hierarchical structure. At its most basic structural level, cellulose chains are arranged in a highly ordered fashion forming crystal units [1, 2], also known as cellulose nanocrystals or nanowhiskers. At the next structural level, cellulose crystals are intercalated with paracrystalline and disordered amorphous domains, forming cellulose microfibrils, which then aggregate to form cellulose bundles or ribbons. The size ranges corresponding to these structural features are largely conditioned by the cellulose native source. For instance, cross-sections of 2-5 nm have been reported for plant-derived cellulose microfibrils [3-8], whereas bacterial and algal cellulose microfibrils typically present larger cross-sections of 4-8 nm [9-11] and greater than 15 nm [12, 13] respectively. In PCWs, cellulose microfibrils are embedded in a multi-component matrix composed of amorphous biopolymers, such as hemicelluloses and pectins. Although these cellulose microfibrils are known to present a key role in controlling growth processes and providing mechanical integrity to PCWs [14-16], many questions still remain with regards to their structure and interactions with matrix components. In addition to its significance in the field of plant biology, understanding the structure of PCWs is also relevant to several industrial sectors such as the production of biofuels, where identification of the structural role of the PCW components and their effect on the digestibility of cellulose are essential to increase processing efficiency [17].

Besides being a major component in PCWs, cellulose is secreted extracellularly by several bacterial species such as *Gluconacetobacter xylinus* (formerly known as *Acetobacter xylinus*), which, when inoculated in a culture medium rich in carbohydrates or polyols,

synthesize a highly hydrated pellicle of cellulose (often referred to as cellulose hydrogel) at the liquid/air interface [18]. Although plant-derived and bacterial cellulose have the same chemical structure, they present quite distinct structural organization due to certain differences in their respective biosynthesis processes. Cellulose biosynthesis is carried out by complex proteins found in the cellular membrane of cellulose-synthesizing organisms, known as terminal complexes (TCs), and the formation of different structural features is assumed to take place sequentially during several synthesis stages [19]. Thus, the architecture of cellulose should be determined by the arrangement of TCs in different organisms and by factors interfering with any of the biosynthesis stages. For instance, TCs in higher plants are arranged into features known as rosettes, which present an hexagonal symmetry; a common assumption therefore is that the number of cellulose chains found in plant-derived microfibrils is divisible by six [4, 20]. On the other hand, TCs are linearly arranged in the cell membrane of *Gluconacetobacter* [19], which has led several researchers to consider bacterial cellulose ribbons as flat objects with rectangular cross-section [21-23], despite no definitive evidence having been provided to support this hypothesis. Furthermore, while bacterial cellulose is synthesized as nearly pure cellulose, interactions between cellulose and matrix components are developed during the PCW biosynthesis process, hence affecting the cellulose assembly pattern. Despite these differences, a number of studies have demonstrated that when PCW biopolymers are added into the *Gluconacetobacter* culture medium, cellulose establishes interactions with the added components, mimicking the assembly of cellulose in PCWs [10, 21, 23-31]. As a result, this has been employed as an efficient approach to investigate the individual role of different PCW components, i.e. avoiding the presence of interfering constituents, in the biosynthesis process and in the properties of the resulting composite materials.

A number of works have investigated the effect of several PCW polysaccharides such as xyloglucan [27, 29, 32], mannans [23, 28] and pectins [21] on the structure of bacterial cellulose by means of microscopic, spectroscopic and diffraction techniques. However, the sample drying typically required by these methods induces significant structural changes in the highly hydrated (ca. 99% H_2O) bacterial cellulose hydrogels[10]. As an alternative, small angle scattering techniques offer a suitable approach to characterise bacterial cellulose hydrogels in their native state, covering a size range from 1 nm to several hundreds of nm. Surprisingly, only a limited number of studies have exploited the potential of SAXS and SANS to investigate the structure of native bacterial cellulose [10, 33-38]. In most of these studies, scattering data have been interpreted in terms of fractal analysis, cross-section estimation, or application of very basic theoretical models which do not account for the complex assembly of cellulose into several structural levels.

The combination of SANS and SAXS with complementary XRD and SEM to characterise bacterial cellulose composites has been recently shown to provide meaningful insights on the differential role of PCW polysaccharides in the cellulose biosynthesis process[10, 17]. In parallel, the development of a suitable theoretical model to describe the scattering arising from hierarchically-assembled pure bacterial cellulose, and its composite hydrogels with two different PCW polysaccharides, is presented here to fully exploit the potential of small angle scattering techniques to the investigation of the interaction mechanisms between cellulose and PCW matrix components.

2. Experimental

2.1 Preparation of pure and composite bacterial cellulose hydrogels

Cellulose only (BC), cellulose/xyloglucan (BC-XG) and cellulose/arabinoxylan (BC-AX) composites were produced following the method described by Mikkelsen et al. [26, 39, 40] with some modifications. In brief, the *Gluconacetobacter xylinus* frozen strain ATCC 53524 (Manassas, VA, USA) was cultivated in Hestrin and Schramm medium at pH 5.0. To produce the BC-XG composites, 1% xyloglucan solution (tamarind xyloglucan, Megazyme International Ireland Ltd., County Wicklow, Ireland) was mixed with double concentrated Hestrin and Schramm medium (1:1) before inoculation, leading to a final xyloglucan concentration of 0.5%. A similar preparation method and concentrations were applied for the culture medium used to synthesize the BC-AX composites [39] (wheat arabinoxylan, Megazyme International Ireland Ltd., County Wicklow, Ireland). Composite hydrogels were cultivated statically at 30°C for 72 hours in 40 mm diameter containers. After cultivation they were harvested and washed 6 times with ice-cold deionised water under agitation at 100 rpm to remove bacteria and excess medium. Samples were stored in 0.02% NaN_3 solution and kept at 4°C until further analysis.

Monosaccharide analysis by GC/MS of washed composite hydrogels showed 27% incorporation of xyloglucan in the BC-XG composite and 53% arabinoxylan in the BC-AX composite. The total solids content in the hydrogels were approximately 0.7% w/v for BC and 1.4% for BC-XG and BC-AX, the remainder being water. Sample thicknesses were measured with a Vernier calliper and were between 0.6 and 1.0 mm.

2.2 Small angle neutron scattering (SANS)

SANS measurements were performed on the 40 m QUOKKA instrument at the OPAL reactor [41]. Three configurations were used to cover a q range of 0.004-0.8 $Å^{-1}$ where q is the magnitude of the scattering vector defined as $q = \frac{4\pi}{\lambda}\sin\theta$ and 2θ is the scattering angle.

These configurations were: (i) source-to-sample distance (SSD) = 20.2 m, sample-to-detector distance (SDD) = 20.1 m, (ii) SSD = 3.9 m, SSD = 4.0 m and (iii) SSD = 10.0 m, SDD = 1.4 m using a wavelength, λ, of 5.034 Å of 10% resolution and with source and sample aperture diameters of 50 mm and 10 mm, respectively. Pure cellulose, and its composite hydrogels, in their fully hydrated state were analysed by placing the samples in sealed 1 mm path length cells with demountable quartz windows and filling the cells with the required solvent (H_2O, D_2O or different H_2O/D_2O mixtures). To maximize the D/H exchange, prior to the SANS measurements, the hydrogels were soaked in D_2O or H_2O/D_2O mixtures with an approximate hydrogel/solvent ratio of 1g/3mL. The samples were initially soaked for 24h and, subsequently, an additional exchange step with fresh solvent was carried out for at least a further 24h. Scattering was measured for a total of 1.25 h for the hydrogels soaked in 60% D_2O and 100% D_2O, and 2.25 h for the hydrogels soaked in H_2O, 20% D_2O and 35% D_2O.

SANS data were reduced using NCNR SANS reduction macros [42] modified for the QUOKKA instrument, using the Igor software package (Wavemetrics, Lake Oswego, OR) with data corrected for empty cell scattering, transmission, and detector and transformed to absolute scale using an attenuated direct beam transmission measurement. To perform the background subtraction, the background contribution in each sample was first assessed by calculating the slope of the linear region at high q on an $I \cdot q^4$ versus q^4 plot. The value of the slope obtained was used to estimate the level of constant background (bulk H_2O, D_2O or different H_2O/D_2O mixtures) which was subsequently subtracted from each sample. All scattering plots presented in this work have been background subtracted by following this procedure. The contrast match point of each sample was determined by plotting the

scattering intensity at a q value of 0.0052 Å^{-1} against the D_2O content of the solvent mixtures (cf. Figure 5A).

2.3 Data analysis

Initial fits to the experimental SANS data of D_2O-soaked hydrogels were conducted by applying a variety of models that have been proposed in the existing literature [33, 35, 38], namely parallelepiped and cylinder with polydisperse radius, within the Igor NIST analysis macro suite [42]. A more sophisticated model, comprising the sum of a power-law term (to account for large-scale structure) plus a core-shell cylinder structure (polydisperse core, fixed thickness shell) was coded by the authors within the same program, and was used as an alternative for fitting the SANS curves for contrast variation experiments.

The function calculated is the following:

$$I(q) = \frac{sf}{V_s} \cdot \sum_{R_s} n(R_c, \sigma_c) \cdot P(q, R_c, R_s, L, SLD_c, SLD_s, SLD_{solv}) + A \cdot q^{-m} + bkg \qquad (1)$$

where the first term corresponds to the form factor of a core-shell cylinder with polydisperse core radius, normalised by multiplying by the number density of particles (sf/V_s), the second term accounts for the power-law behaviour and the third term corresponds to the incoherent background remaining after the solvent background subtraction (which in this case was close to zero). Since the SANS data were collected on an absolute scale, the scale factor parameter should correspond to the volume fraction of cylindrical particles. This value relies on detailed knowledge of the thickness of the sample.

The form factor of the core-shell cylinder is calculated by the following equation:

$$P(q, R_c, R_s, L, SLD_c, SLD_s, SLD_{solv}) = \int_0^{\pi/2} \sin\theta \cdot d\theta \cdot \left[V_s(SLD_s - SLD_{solv}) \frac{\sin\left(\frac{qL\cos\theta}{2}\right)}{\frac{qL\cos\theta}{2}} \cdot \frac{2J_1(qR_s\sin\theta)}{qR_s\sin\theta} + V_c(SLD_c - SLD_s) \frac{\sin\left(\frac{qL\cos\theta}{2}\right)}{\frac{qL\cos\theta}{2}} \cdot \frac{2J_1(qR_c\sin\theta)}{qR_c\sin\theta} \right]^2 \quad (2)$$

where R_c is the core radius, R_s is the shell radius ($R_s = R_c + t_s$), t_s is the radial shell thickness, L is the cylinder length, V_c is the core volume ($V_c = \pi R_c^2 L$), V_s is the shell volume ($V_s = \pi R_s^2 L$), J_1 is the first order Bessel function and θ is the angle between the cylinder axis and the scattering vector q.

Additionally, the polydispersity of the core radius, σ_c, is modelled using a log-normal distribution:

$$n(R_c, \sigma_c) = \frac{exp\left(-\frac{1}{2}\left[\frac{ln(R_c/R_0)}{\sigma_c}\right]^2\right)}{\sqrt{(2\pi)}\sigma_c R_c} \quad (3)$$

where R_0 is the mean core radius.

This model is thus defined by eleven parameters: scale factor (sf), R_c, L, σ_c, t_s, SLD (scattering length density) of the core (SLD_c), SLD of the shell (SLD_s), SLD of the solvent (SLD_{solv}), power-law coefficient (A), power-law exponent (m) and incoherent background (bkg).

When fitting the SANS contrast variation experimental data, two new variables, x_{core} and x_{shell} were created to describe the volume fraction of cellulose present in the core and the shell of the ribbons, respectively. Considering the situation of hydration in a 100% D_2O solvent, and assuming that both the core and shell regions may be occupied only by cellulose

and water then these variables are directly related to the SLD of the core and the shell as follows:

$$SLD_{core} = x_{core} \cdot \left[SLD_{cell} + degex_{cell\ core} \cdot \left(SLD_{cell\ full\ exch} - SLD_{cell}\right)\right] + (1 - x_{core}) \cdot \left[SLD_{bound\ H2O} + degex_{solv\ core} \cdot (SLD_{bound\ solv} - SLD_{bound\ H2O})\right] \quad (4)$$

$$SLD_{shell} = x_{shell} \cdot \left[SLD_{cell} + degex_{cell\ shell} \cdot \left(SLD_{cell\ full\ exch} - SLD_{cell}\right)\right] + (1 - x_{shell}) \cdot \left[SLD_{bound\ H2O} + degex_{solv\ shell} \cdot (SLD_{bound\ solv} - SLD_{bound\ H2O})\right] \quad (5)$$

where $degex_{cell\ core}$ and $degex_{cell\ shell}$ represent the degree of H/D exchange in the cellulose fraction present within the core and shell, respectively and $degex_{solv\ core}$ and $degex_{solv\ shell}$ correspond to the degree of exchange undergone by the solvent contained within the core and shell, respectively. These four parameters, which take a value between zero and unity, represent the extent to which exchange has occurred in both the cellulose and solvent with respect to the maximum possible SLD values for each fully exchanged component. Thus SLD_{cell} and $SLD_{cell\ full\ exch}$ correspond to the SLD of non-exchanged and fully exchanged cellulose, respectively and $SLD_{bound\ H2O}$ and $SLD_{bound\ solv}$ are the SLD values of the tightly bound water initially found within the cellulose ribbons and the SLD of tightly bound solvent (i.e. associated with the corresponding solvent used for the contrast variation experiments) and both based on a density increase of 25% as reported in [43, 44].

Thus, the final model was defined by the following nineteen parameters: sf, R_c, L, σ_c, t_s, x_{core}, x_{shell}, $degex_{cell\ core}$, $degex_{cell\ shell}$, $degex_{solv\ core}$, $degex_{solv\ shell}$, SLD_{cell}, $SLD_{cell\ full\ exch}$, SLD_{solv}, $SLD_{bound\ solv}$, $SLD_{bound\ H2O}$, A, m and bkg. From these nineteen parameters, the following nine were fixed: L, σ_c, $degex_{solv\ shell}$, SLD_{cell}, $SLD_{cell\ full\ exch}$,

SLD_{solv}, $SLD_{bound\ solv}$, $SLD_{bound\ H2O}$ and bkg. Of the remaining ten parameters, eight parameters: sf, R_c, t_s, x_{core}, x_{shell}, $degex_{solv\ core}$, $degex_{cell\ core}$ and $degex_{cell\ shell}$, were constrained between values consistent with known sample properties.

Regarding the morphological parameters of the samples, the cylinder length was fixed to a value of 500 nm, which is in agreement with values previously reported for the length of crystalline cellulose [45]. In addition, the cylinder length beyond this has limited effect on the low q scattering. The polydispersity of the core radius, equivalent to the polydispersity of the ribbon thickness since the shell thickness was considered to be constant, was fixed to 0.2; the latter corresponds to the approximate relative error obtained when measuring the ribbon thickness from SEM micrographs [10]. The core radius and the radial shell thickness were constrained to refine between values of 3 and 30 nm; these values were based on consideration of the minimum cellulose crystallite dimensions and the maximum ribbon width, estimated in previous work [10].

The scale factor was estimated, before fitting, to be within the range of 0.004-0.015; this was based on uncertainties concerning the sample thickness (0.6-1.0 mm) and knowledge of the dry weight (0.7-1.4%). To account for possible thickness or dry weight measurement errors, the scale factor was allowed to vary between 0.001 and 0.03 during the fitting process. In the particular case of the solvent mixture closest to the contrast match point (i.e. samples soaked in 33% D_2O), where the SLD contrast between the solvent and the crystalline cellulose is negligible, this parameter was fixed to a value of 0. The core and shell cellulose volume fractions were constrained between 0 and 1. The solvent contained within the shell was assumed to be completely exchanged (i.e. the solvent exchange within the shell was fixed to a value of 1). On the other hand, the cellulose H/D exchange for both core and shell regions

and the solvent exchange within the core were allowed to refine between 0 and 1 (i.e. no exchange and complete exchange).

The SLD of fully exchanged cellulose was calculated for each solvent mixture considering that a value of $3.66 \cdot 10^{10}$ cm^{-2} would be obtained if complete exchange of labile hydroxyl groups occurred when soaking the samples in 100% D_2O, whereas a value of $1.87 \cdot 10^{10}$ cm^{-2} would correspond to 100% H_2O (i.e. no H/D exchange) (cf. Table 1). The tightly bound solvent SLD values were calculated for solvent composition based on an increase of 25% in the physical density. The bulk solvent SLD values were re-calculated based on consideration of the sample/solvent ratio used for the two successive exchange steps. Thus, for instance, one bacterial cellulose sample weighing ca. 14.7 g soaked in 40 mL of pure D_2O should result in a final solvent composition of ca. 75% D_2O viz. 14.7g sample = 1.03g cellulose + 13.67mL H_2O, in 40 mL of D_2O. Assuming that complete solvent exchange occurs during the first exchange step, the final solvent composition would be around 93% D_2O (1.03g cellulose + 10.25mL D_2O + 3.42mL H_2O + 40mL D_2O), with a corresponding neutron SLD value of $5.89 \cdot 10^{10}$ cm^{-2}. By following the same procedure, the final solvent compositions when soaking the samples in 60%, 35% and 20% D_2O solutions were calculated as 56%, 33% and 18% D_2O, and having SLD values of $3.33 \cdot 10^{10}$ cm^{-2}, $1.73 \cdot 10^{10}$ cm^{-2} and $0.69 \cdot 10^{10}$ cm^{-2}, respectively.

2.4 Small angle X-ray scattering (SAXS)

SAXS measurements of the native pure cellulose and composite hydrogels (soaked in excess H_2O) were performed on a Bruker Nanostar instrument, as described previously [10]. The SAXS patterns were fitted using the same power-law plus core-shell function applied to fit the SANS data. However, in the case of X-rays, the scattering intensity arises mainly from

the contrast between the interior of the crystalline cellulose microfibrils (i.e. the core, according to the applied model described above) and the surrounding hydrated paracrystalline cellulose exterior region (i.e. the shell). Thus, the SLD values of the core and the shell were expressed as follows:

$$SLD_{core} = SLD_{cryst\ cell} \tag{6}$$

$$SLD_{shell} = (x_{shell} \cdot SLD_{paracryst\ cell}) + ((1 - x_{shell}) \cdot SLD_{bound\ H2O}) \tag{7}$$

where x_{shell} corresponds to the cellulose volume fraction in the microfibril exterior region and $SLD_{cryst\ cell}$, $SLD_{paracryst\ cell}$ and $SLD_{bound\ H2O}$ are the SLD values of the crystalline cellulose, the paracrystalline cellulose and the tightly bound water, respectively (cf. Table 1). Hence, in the particular case of applying the core-shell model to describe the structure of the individual cellulose microfibrils, the fitting function is described by a total of twelve parameters, from which six were fixed (L, $SLD_{cryst\ cell}$, $SLD_{paracryst\ cell}$, SLD_{solv}, $SLD_{bound\ H2O}$ and bkg), four were constrained (sf, R_c, σ_c and x_{shell}) and only two parameters were refined without any constraint (A and m). Based on the dry weight of the samples and considering possible dry weight measurement errors, as well as the possible reduction in the sample water content as a consequence of squeezing the hydrogel through the 1 mm capillary, the scale factor was constrained between 0.001 and 0.1. The core radius was constrained to refine between values of 1 and 30 nm, whereas the polydispersity of the core radius and the cellulose volume fraction within the shell were constrained between 0 and 1.

Table 1. Neutron and X-ray SLDs for the different polysaccharides and solvents used in the SANS experiments. The following physical densities were used: ρ(crystalline cellulose) = 1.60 g/cm^3 [43], ρ(paracrystalline cellulose) = 1.51 g/cm^3 [46], ρ(amorphous cellulose) = 1.48 g/cm^3 [47], ρ(arabinoxylan) = 1.40 g/cm^3, ρ(xyloglucan) = 1.40 g/cm^3 [48]. Bound H_2O and D_2O SLDs were calculated assuming a density increase of 25% with respect to the bulk, as reported in [43, 44].

	Neutron SLD (10^{10} cm^{-2})	X-ray SLD (10^{10} cm^{-2})
Cellulose (crystalline)	1.87	14.46
Cellulose (crystalline, D_2O exchanged)	3.66	---
Cellulose (paracrystalline)	1.77	13.65
Cellulose (paracrystalline, D_2O exchanged)	3.46	---
Cellulose (amorphous)	1.73	13.38
Cellulose (amorhpous, D_2O exchanged)	3.39	---
Arabinoxylan	1.62	12.64
Xyloglucan	1.62	12.65
Bulk H_2O	-0.56	9.47
Bound H_2O	-0.70	11.84
Bulk D_2O	6.38	---
Bound D_2O	7.97	---

3. Results and discussion

3.1 Model development: Fitting of bacterial cellulose SANS data

Bacterial cellulose hydrogels are structurally complex systems which have been characterized by SANS in a very limited number of works [10, 35, 37]. To date, attempts to describe the experimental SANS data have been carried out based on unrealistic models which do not account for the real complexity of the system and, consequently, have not been able to satisfactorily fit the experimental data over the relevant intensity and q range. The aim of this work is to assess the validity of a more complex model, based on the prior knowledge of the system, to describe the SANS data of pure and composite hydrogels. Note that throughout this paper, the experimental data and associated fitting functions are illustrated on a logarithmic (as opposed to linear) scale of both intensity and q as this provides a clear demonstration of the quality, or otherwise, of the fitting functions; in addition, and unusual for small-angle scattering data from polymeric systems, a reduced χ^2 value is also provided.

The SANS patterns of pure bacterial cellulose hydrogels and its composites with arabinoxylan and xyloglucan have been previously shown to consist of the following three distinct regions: (1) low q region ($q < 0.01$ Å^{-1}) dominated by interfacial surface scattering (i.e. arising from the interface between the cellulose ribbons and the surrounding bulk solvent) and evidenced by a power-law behaviour; (2) appearance of one or two characteristic shoulders in the region of $q = 0.01$-0.08 Å^{-1}; and (3) a high q region ($q > 0.15$ Å^{-1}) dominated by incoherent background scattering arising from the hydrogenous material [10]. To explain the observed scattering patterns, a range of models, including those previously proposed in the literature, have been applied in the present work.

The small angle scattering data of bacterial cellulose samples have been typically fitted using one-phase models, accounting for a single solid phase surrounded by bulk solvent [33, 35, 38]. Bacterial cellulose ribbons present a morphology of long entangled objects with cross-

sectional dimensions within the range of 20-60 nm [11, 21-23, 49]. Although the length of each ribbon has not been unambiguously determined, they have been seen to be periodically twisted with an approximate repeating distance of 1 μm [22]; the cellulose crystallites composing the ribbons have been determined to present lengths of ca. 400-600 nm [45]. On the other hand, there is scarce information regarding the cross-sectional shape of the ribbons. On the basis of the linear arrangement of TCs in the bacterial cell membrane [19] and on the observation of thick and thin regions in the SEM and TEM images of bacterial cellulose samples, which have been considered to arise from the periodical twisting of flat ribbons along their axis [21-23], it is commonly assumed that bacterial cellulose possesses a flat ribbon-like structure [33, 38, 50]. According to this, the cellulose microfibril and ribbon dimensions have been estimated from SAXS experiments by calculating the radius of gyration and the cross-sectional area. Whereas Astley et al. reported a microfibril cross-section of 1 nm x 16 nm [33], Tischer et al. estimated ribbon dimensions of 7 nm x 70 nm [38]. Assuming such microfibril and ribbon dimensions, theoretical scattering curves have been obtained by using a parallelepiped model and the results, together with the experimental data, are displayed in Figure 1. It is evident that consideration of the microfibril cross-section values, i.e. 1 nm x 16 nm, does not provide acceptable description of the experimental data (reduced χ^2 value = 47.1). This is unsurprising as, even in their hydrated state, bacterial cellulose microfibrils are aggregated into larger structures, i.e. ribbons. Although the fitting curves produced by using the ribbon dimensions extracted from literature provide a much better approximation to the experimental curve (reduced χ^2 = 27.2), the shoulder feature reproduced by the theoretical curve does not appear in the q range of interest, as observed in the corresponding Kratky plot (Figure 1B). To account for the ribbon thickness (i.e. the cross-sectional dimension observed in the microscopy images), which was previously determined for the bacterial cellulose hydrogels used in the present work to be around 35 nm [10], the parallelepiped model was also

applied by initially setting the ribbon thickness to a value of 35 nm and allowing it to vary between 6 and 60 nm (based on the reported values for the minimum cellulose crystallite dimensions and the maximum ribbon width [10] as detailed in section 3.2), with the best 'agreement' to the experimental data obtained for a parallelepiped cross-section of ca. 4.9 nm x 55.3 nm. The reduced χ^2 value associated with the 'fit' was 19.2, reflecting only a slight improvement with respect to refining the 7 x 70 nm parallelepiped dimensions. Furthermore, as observed in Figure 1A, the parallelepiped model was still unable to accurately reproduce the experimental scattering data over the considered q range and the theoretical curves presented a characteristic feature in the region of q = 0.1 - 0.3 $Å^{-1}$, which arose from the shortest parallelepiped edge, i.e. the ribbon width. The fact that such a feature was not detected in the experimental curve, indicates that the parallelepiped model may not be the most appropriate to describe the SANS data of bacterial cellulose hydrogels.

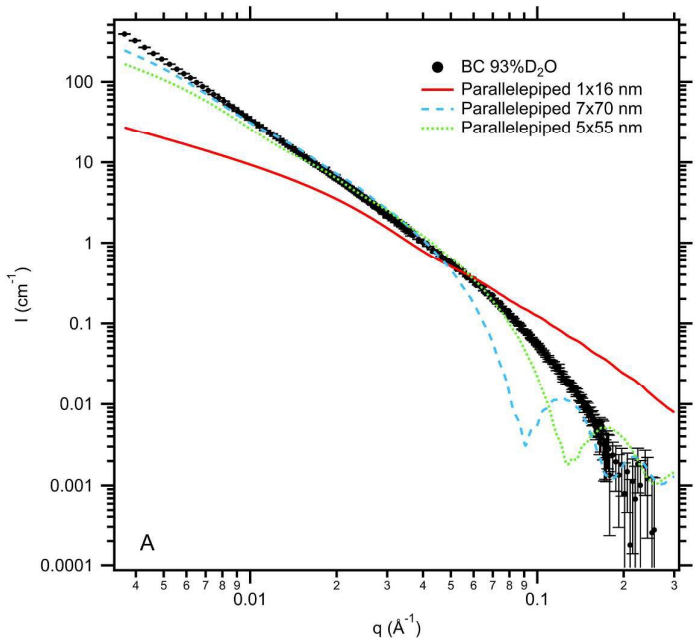

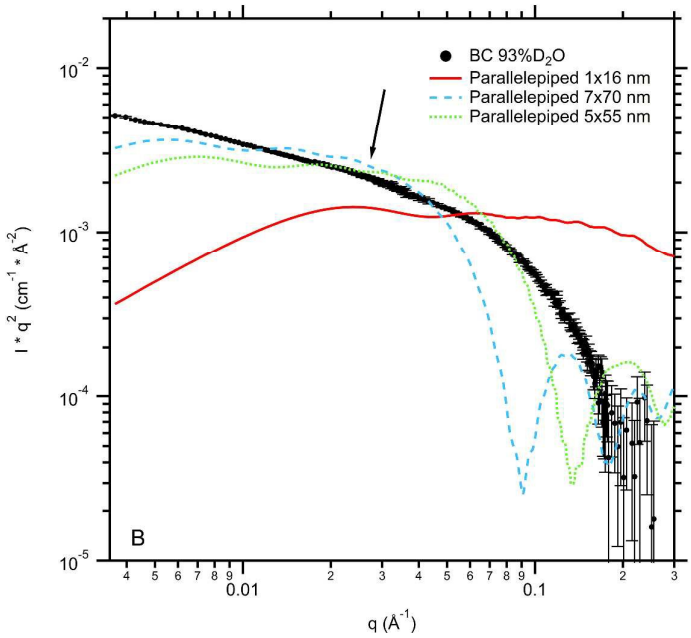

Figure 1. (A) SANS experimental data and corresponding model curves for the BC hydrogel (soaked in D_2O). Dots represent the experimental data and lines show the fits obtained using a parallelepiped model. The following parameters were considered for each fitting procedure: The scale factor was allowed to vary between 0.001 and 0.03, the longest parallelepiped edge was fixed to 500 nm, the SLD of the parallelepiped was allowed to vary between $1.87 \cdot 10^{10}$ cm^{-2} ($SLD_{crystalline\ cellulose}$) and $5.89 \cdot 10^{10}$ cm^{-2} ($SLD_{solvent}$) and the SLD of the solvent was fixed to $5.89 \cdot 10^{10}$ cm^{-2} (assuming complete solvent exchange, final solvent composition is ca. 93% D_2O). Different ribbon cross-sections were considered by fixing or constraining the shortest and medium edges as follows: (1) fixed to 1 nm and 16 nm, respectively (red line), (2) fixed to 7 nm and 70 nm, respectively (blue line) and (3) constrained between 1 and 60 nm and between 6 and 60 nm, respectively (green line). (B) Corresponding Kratky plots; the appearance of the shoulder-like feature in the experimental data is indicated by an arrow.

With the aim of approaching the sheet-like morphology observed in the cross-section of dried bacterial cellulose samples, a large disk model, approximated by a cylinder with radius of ca. 116 nm and thickness of ca. 8 nm, was previously used to fit the SANS patterns of deuterated bacterial cellulose [35]. Although acceptable fits were reported by using this approach, it should be noted that a high radius polydispersity of ca. 0.95 was assumed. Furthermore, the model considered the disk radius, which accounts for the ribbon thickness, to be significantly larger than the values of 20-60 nm typically reported for native bacterial cellulose; it is more likely to correspond to the aggregates of ribbons that are usually formed as a consequence of the drying process. To assess the adequacy of this model, the fitting parameters were allowed to vary within the range of values known to be consistent with the BC sample analysed in the present work and compared to the result when setting the values considered by He et al. [35]. As shown in Figure 2, the large disk model presented similar issues to that of the parallelepiped, i.e. a feature characteristic of the shortest ribbon dimension (the ribbon width) was observed at q values of approximately 0.11 $Å^{-1}$ and the model did not appear to reproduce correctly the shoulder located at lower q values in the experimental data (reduced χ^2 = 33.4 and 31.6 for the large disk model when fixing and refining the disk radius values respectively).

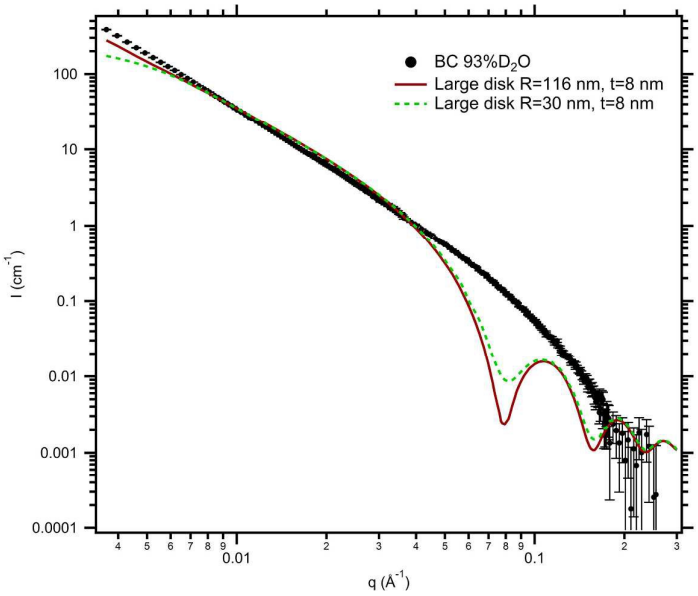

Figure 2. SANS experimental data and corresponding model curves for the hydrated BC hydrogel (soaked in D_2O). Dots represent the experimental data and dashed lines show the 'fits' obtained using a large disk model. The following parameters were considered for each fitting procedure: The scale factor was allowed to vary between 0.001 and 0.03, the cylinder length was fixed to 8 nm, the SLD of the parallelepiped was allowed to vary between $1.87 \cdot 10^{10}$ cm^{-2} ($SLD_{crystalline\ cellulose}$) and $5.89 \cdot 10^{10}$ cm^{-2} ($SLD_{solvent}$) and the SLD of the solvent was fixed to $5.89 \cdot 10^{10}$ cm^{-2}. Two different cylinder radii were considered by fixing or constraining the radius and polydispersity as follows: (1) fixed to 115.8 nm and 0.95, respectively (red dashed line) and (2) constrained between 3 and 30 nm and 0.2 and 0.95, respectively (green dashed line).

An alternative to the rectangular cross-section could be based on the consideration of bacterial cellulose ribbons as cylindrical objects. Indeed, looking at the interwoven morphology of the bacterial cellulose hydrogels previously observed by SEM [10, 51], a cylindrical cross-section seems plausible. Data fitting by considering such morphology, with a polydisperse radius between 3-30 nm is shown in Figure 3. Although the cylindrical

model had the effect of eliminating the undesired peak obtained with the rectangular cross-section, it still did not lead to an acceptable fit (reduced $\chi^2 = 60.7$). Taking into account that the low q region ($q < 0.01$ Å^{-1}) is expected to be dominated by the interfacial scattering between the network of interwoven cellulose ribbons and the solvent as indicated from previous microscopy characterisation [10, 51], the addition of a power-law term into the model is not only physically necessary but improves the fits over the region corresponding to larger structural features (Figure 3A), as confirmed by the reduced χ^2 value of 14.0; however, the sum model was still not able to reproduce the shoulder appearing in the experimental scattering data, as clearly seen in the Kratky plot (Figure 3B).

All the models considered thus far assume that bacterial cellulose ribbons may be described as solid objects with a particular shape. Nevertheless, it is known that the ribbons are actually composed of several microfibrils that interact by hydrogen bonding [11]. The exact cross-sectional shape of cellulose microfibrils has not been determined but they are thought to contain a crystalline interior of ca. 3-8 nm width [9, 10, 38] and a paracrystalline exterior region with increased chain packing and hydrogen bonding disorder [4]. It should be noted that the cited works refer to plant-derived cellulose microfibrils and, to date, it has not been confirmed whether bacterial and plant-derived cellulose microfibrils present a similar structure. Nevertheless, the cross-section decrease reported when subjecting bacterial cellulose to an acid hydrolysis treatment [45] suggests that the surface disorder induced towards the exterior of the microfibrils is plausible for the case of bacterial cellulose. Whereas the crystallites are assumed to be impermeable to solvents, several works have suggested that a certain amount of water is present covering the crystallites' surface [33, 50, 52]. This interfibrillar water is probably bound to the hydroxyl groups found in the disordered cellulose chains in the paracrystalline regions and therefore likely to present

a different behavior to that of the bulk-like water filling the voids found within the network of interwoven ribbons. Based on these structural characteristics, one may hypothesize that bacterial cellulose ribbons can be considered as two-phase systems composed of a core and a shell presenting different solvent accessibility [10] viz. (i) an inner region containing solvent-impermeable crystallites, surrounded by paracrystalline cellulose and water, the latter being associated by a dense network of hydrogen bonding and (ii) paracrystalline cellulose and water composing the outer / surface region of the ribbons. Assuming such a model has merit, it would imply that when bacterial cellulose hydrogels are soaked in D_2O, the water held in the paracrystalline fraction might be gradually exchanged, although this process would be partially obstructed by the hydrogen bonding network present in the core of the ribbons. Based on this, a core-shell formalism has been suggested to describe the SANS data of bacterial cellulose and its composites with arabinoxylan and xyloglucan [10]. The combination of this model with power-law scattering describes the experimental data well as further evaluated by the Kratky plot displayed in Figure 3B and as indicated by the significantly lower reduced χ^2 value of 7.6 associated with the attained fit. This, together with the fact that the core-shell formalism provides a physical description consistent with what is known about the structure of hydrated bacterial cellulose, highlights the potential of this model to describe the experimental SANS data. It should be considered that although the SANS structural features here shown are relatively weak, the utilisation of such a rather complex model has been previously justified as it was able to accurately reproduce the experimental data of pure and composite hydrogels which showed much stronger shoulder-like features in their associated scattering patterns [10]. Comparison of the fitting parameters obtained for the previously analysed hydrogels with those obtained in the present work, suggests that the different intensity of the structural features within hydrogel batches may be related to a densification effect. The strongly featured cellulose

hydrogel presented greater core and shell SLD values (SLD_{core}=5.58·10^{10} cm^{-2} and SLD_{shell}=7.92·10^{10} cm^{-2}) than the cellulose hydrogel characterised in this work, suggesting that the stronger structural features arise from an increased solvent accessibility in the less dense hydrogel structures. However, the effect of harvesting parameters on the properties of the synthesized cellulose hydrogels is out of the scope of this manuscript and will be thoroughly investigated elsewhere.

Incorporating a gradation in the SLD of the three different phases considered by the model (i.e. core, shell and solvent) may lead to a further improvement of the attained fit although this would naturally complicate the fitting function with the requirement of additional refinable parameters to describe the SLD 'roughness'. However, it should also be mentioned that application of a power-law plus core-shell parallelepiped model did not lead to an improved description of the experimental data (as indicated by the reduced χ^2 value of 7.8), as assuming a rectangular cross-section led to the appearance of undesired features arising from the parallelepiped shortest dimension, similar to the simpler parallelepiped and large disk models above (cf. Figure S1).

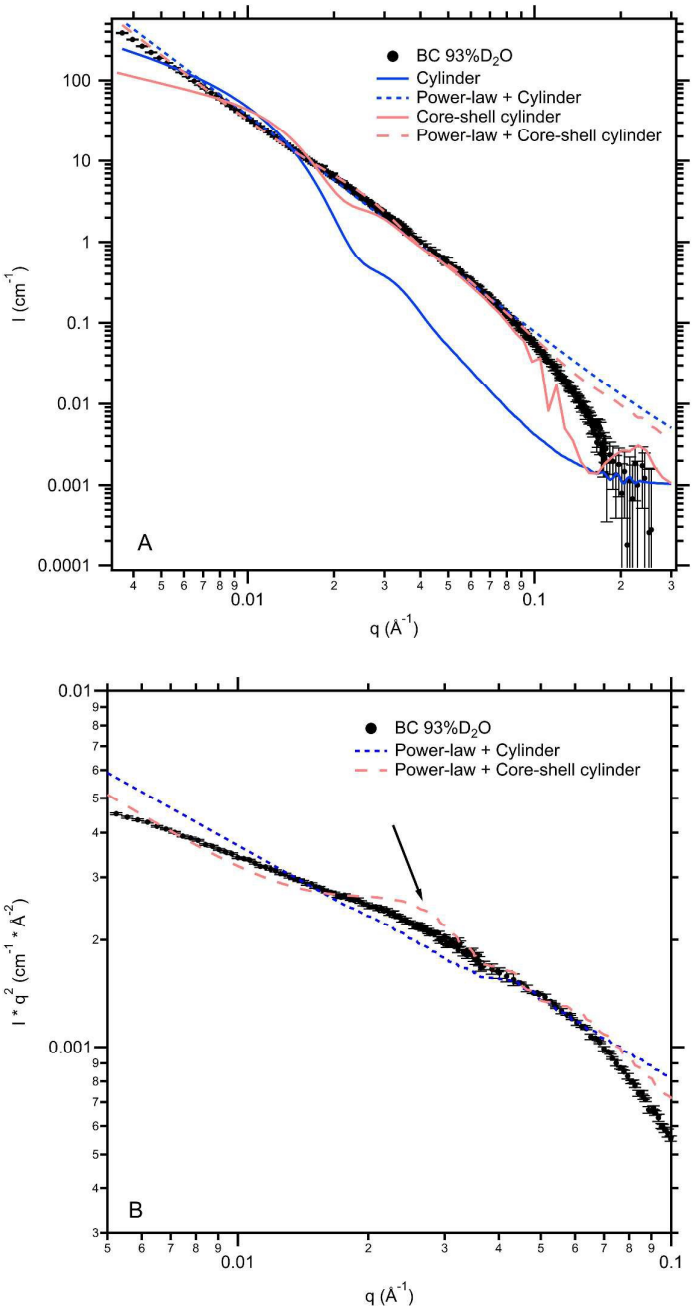

Figure 3. (A) SANS experimental data and fits for the hydrated BC hydrogel (soaked in D_2O). Dots represent the experimental data and lines show the fits obtained using different models assuming a circular cross-section. (1) Cylinder with polydisperse radius (blue continuous line), (2) sum of a power-law plus cylinder with polydisperse radius model (blue dashed line), (3) core-shell cylinder with polydisperse radius (red continuous line) and (4) sum of a power-law plus a core-shell cylinder with polydisperse radius (red dashed

line). In all the cases the scale factor was constrained between 0.001 and 0.03, the cylinder length was fixed to 500 nm and the SLD of the solvent was fixed to $5.89 \cdot 10^{10}$ cm^{-2}. (B) SANS Kratky plot comparing the cylinder and core-shell sum models within the q region of interest, where the characteristic shoulder feature observed in the experimental data is indicated by an arrow.

Table 2. Parameters obtained from the fits of the different models considered assuming a cylindrical morphology.

	Cylinder		Core-shell cylinder	
Scale factor	0.004	0.001	0.030	0.066
Radius (nm)	15.00	15.00	19.08	10.18
Cylinder length (nm)	500 (*)	500 (*)	500 (*)	500 (*)
Polydispersity	0.2 (*)	0.2 (*)	0.2 (*)	0.2 (*)
$SLD_{cylinder/core}$ (10^{10} cm^{-2})	2.70	5.97	4.45	4.03
SLD_{shell} (10^{10} cm^{-2})	---	---	7.97	7.63
$SLD_{solvent}$ (10^{10} cm^{-2})	5.89 (*)	5.89 (*)	5.89 (*)	5.89 (*)
Radial shell thickness (nm)	---	---	3.90	3.95
Power-law coefficient	---	$1.61 \cdot 10^{-4}$	---	$9.71 \cdot 10^{-5}$
Power-law exponent	---	2.68	---	2.75

Parameters fixed during the fitting process are displayed with (*).

3.2 Model validation: Global fitting of SANS contrast variation experiments

To further test the validity of the model (core-shell cylinder with polydisperse radius plus power-law), the experimental SANS data of pure and composite bacterial cellulose hydrogels soaked in different D_2O/H_2O solvent mixtures were simultaneously fitted. As

described in section 2.4, the sum model is characterised by eleven parameters; however, to obtain more direct information from the fitting process, the model was defined as a function of the cellulose volume fraction and the cellulose and solvent H/D exchange in the core and the shell, which are directly related to the core and shell SLDs, as defined by equations (4) and (5). This model, defined by nineteen parameters, was applied to fit the SANS contrast variation experimental data of BC, BC-AX and BC-XG samples and the results are displayed in Figures 4A, 4B and 4C. It may be observed that, despite the relatively broad q range considered for the fitting process, the proposed model provided relatively good fits for the three different samples, with corresponding values for the reduced χ^2 of 16.8, 23.8 and 18.6 for the BC, BC-AX and BC-XG samples, respectively. The parameters obtained with the best simultaneous fits for the pure and composite bacterial cellulose hydrogels are summarised in Tables 3a, 3b and 3c. It is worth noting that, as deduced from the values listed in the tables, fitting of the experimental data with the developed model led to physically realistic values for the variables describing the mathematical function.

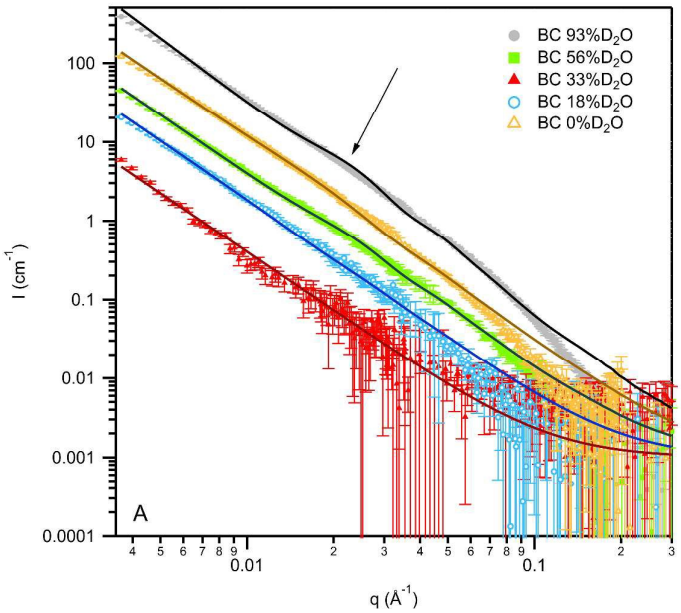

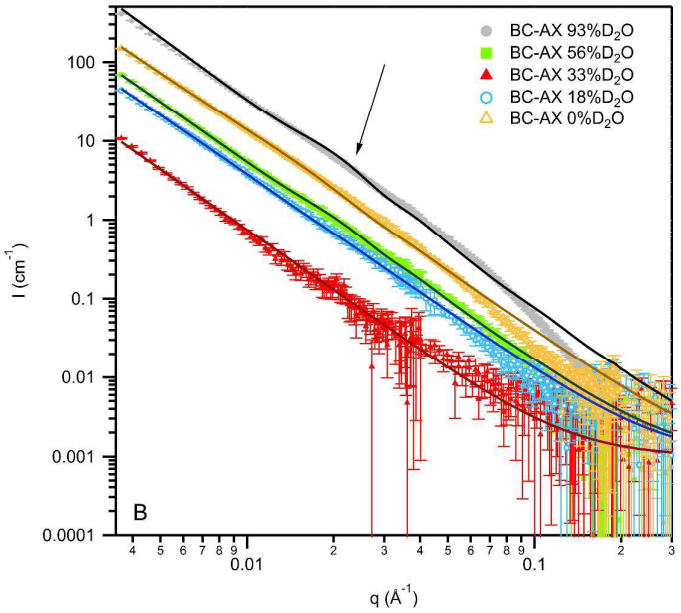

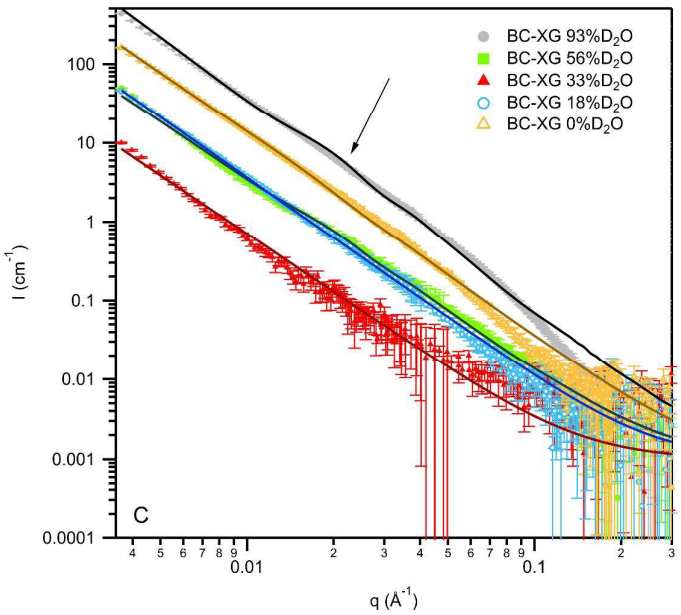

Figure 4. SANS patterns for solvent contrast variation experiments on BC (A), BC-AX (B) and BC-XG (C) hydrogels. Dots represent the experimental data, whereas the solid lines correspond to the best global fits obtained using the power-law plus core-shell cylinder model. The shoulder features detected in the experimental data are indicated with arrows.

Careful analysis of the obtained fitting parameters was carried out with the aim of extracting information regarding the structure of the different analysed materials; Figure 7 illustrates the so-obtained ribbon representation for the pure and composite hydrogels. As already mentioned, the fitting function comprises the sum of a power-law model plus a core-shell cylinder form factor. Whereas this latter term corresponds to the form factor of the cellulose ribbons, the power-law term is added to account for the larger scale structure, i.e. the network of randomly oriented ribbons that are forming the cellulose hydrogel. The contribution from the larger-scale structure is weighted by the power-law coefficient and therefore, greater coefficient values are indicative of the scattering intensity being more strongly affected by the larger scale structure. Indeed, as observed in Tables 3a, 3b and 3c, when the volume of D_2O in the solvent is close to the theoretical contrast match point of cellulose (i.e. 33% D_2O), the power-law coefficient reaches its minimum value. On the other hand, when the contrast between the surface of the ribbons and the surrounding bulk solvent is maximum (i.e. 93% D_2O), the coefficient reaches its maximum value. Interestingly, whereas at 33% D_2O the pure cellulose hydrogel and the BC-XG hydrogel present a power-law exponent close to -2.5, the BC-AX hydrogel presents a greater power-law exponent of -2.6. This may indicate a more 'visibly' branched structure for the composite BC-AX hydrogel when the cellulose crystalline fraction is approximately matched out due to the presence of the amorphous arabinoxylan coating the cellulose ribbons' surfaces.

The overall ribbon cross-section, calculated from the core radius and shell thickness, does not seem to be strongly affected by the incorporation of arabinoxylan and xyloglucan into the system, and the estimated dimensions (ca. 33.6 nm, 41.6 nm and 41.8 nm for BC, BC-

AX and BC-XG, respectively) are within the range previously determined by SEM characterisation (35.5 ± 9.1 nm, 32.1 ± 7.2 nm and 36.5 ± 8.4 nm for BC, BC-AX and BC-XG, respectively) [10]. Furthermore, while the relative thickness of the shell is approximately constant when xyloglucan is incorporated into the system (ca. 33% with respect to the total ribbon cross-section), a thicker shell (ca. 39%) is induced by the presence of arabinoxylan. This may suggest that the arabinoxylan is preferentially located within the accessible ribbon surface, hence increasing the relative thickness of the shell.

As expected, due to the limited solvent accessibility (i.e. limited solvent diffusion towards the inner region of cellulose ribbons) caused by the strong hydrogen bonding network, the apparent cellulose volume fraction in the ribbons' core is larger than in the shell for all the samples. In the pure and composite hydrogels, the shell region is mostly composed of bound solvent, with only a 0.1-0.2% cellulose volume fraction. Interestingly, the composite BC-XG hydrogel shows a decreased cellulose volume fraction within the core (ca. 21% cellulose), as compared with that of the pure cellulose hydrogel (ca. 23% cellulose), whereas the opposite effect is observed for the BC-AX hydrogel (with ca. 27% cellulose). A reduction in the cellulose volume fraction may be due to either an increased amount of solvent and/or to the presence of PCW polysaccharides within the ribbons' core. This result indicates that whereas xyloglucan is expected be located within the ribbons' core, hence reducing the corresponding cellulose volume fraction, arabinoxylan might be preferentially located on the surface of the ribbons, leading to a reduced amount of solvent contained within the ribbons' core. Such different behaviour suggests that strong cellulose-xyloglucan interactions are established at the microfibril structural level, whereas the cellulose-arabinoxylan interactions seem to be limited to the surface of the ribbons.

In addition, the model is able to provide information regarding the extent to which the cellulose and solvent fractions contained within the core and the shell of the ribbons are exchanged when soaking the samples in different H_2O/D_2O mixtures. Assuming that the shell is easily accessed by the fresh solvent used to soak the samples, it is reasonable to expect the solvent contained within the shell to be completely exchanged (thus the solvent exchange within the shell was fixed to a value of 1 during the fitting procedure). Interestingly, the solvent exchange within the core is around 58-60% for the pure cellulose and the BC-AX hydrogel, while a greater value of ca. 68% corresponds to the BC-XG hydrogel. This is in agreement with the presumed existence of a dense network of hydrogen bonded cellulose/water in the ribbons' core and suggests that approximately 42-32% of the water tightly bound to the cellulose paracrystalline fraction is not exchanged. The decreased amount of tightly bound water induced by the presence of xyloglucan in the BC-XG composite hydrogel suggests a greater solvent access towards the inner region of the cellulose ribbons, in agreement with the reduced cellulose volume fraction attained for this sample. Solvent accessibility towards the ribbons' core may be promoted by (i) the presence of additional hydroxyl groups provided by the PCW polysaccharides and/or (ii) the existence of a weaker hydrogen bonding network due to the establishment of cellulose-PCW polysaccharide interactions. Although the amount of xyloglucan in the BC-XG hydrogel is almost half of the amount of arabinoxylan in the BC-AX hydrogel, only the former presents a significant effect in promoting solvent accessibility towards the ribbons' core. Different batches of pure and composite hydrogels also showed an increased solvent accessibility promoted by the presence of PCW polysaccharides, this effect being more obvious for the hydrogel containing xyloglucan [10]. This observation was hypothesised to be a consequence of the ability of xyloglucan to interact with the individual cellulose microfibrils contained within the ribbons' core, whereas arabinoxylan-cellulose

interactions are limited to the ribbons' surface. Complementary XRD analyses have demonstrated that the incorporation of xyloglucan promotes the creation of fewer crystalline and I_β-rich cellulose microfibrils [10], thus supporting the hypothesis of a close association between the cellulose microfibrils and xyloglucan.

With regards to the cellulose component, the fitting results support the hypothesis of a shell mainly composed of paracrystalline or accessible cellulose, with exchangeable hydroxyl groups, and a core containing a fraction of non-accessible crystalline cellulose (as suggested by the ca. 1 and 0.7 cellulose exchange values, within the shell and core of the pure cellulose hydrogel, respectively). Note that although the cellulose exchange within the shell tends towards unity, large standard deviation values are associated with this parameter, due to its weak contribution to the SLD value of the highly hydrated shell (with only 0.1% cellulose). Previous dynamic vapour sorption measurements of freeze-dried bacterial cellulose sheets exposed to a D_2O atmosphere indicated that 1.24 out of 3 labile hydroxyl groups from each glucose monomer are exchanged [53]. This would imply a cellulose exchange of ca. 41%, which is considerably lower than the complete exchange obtained here for the ribbons' shell (i.e. the accessible region). It has been previously demonstrated that drying processes reduce strongly the ability of bacterial cellulose hydrogels to rehydrate [54], which is mainly due to the creation of strong interfibrillar hydrogen bonds when moisture is removed from the system. It would therefore be reasonable to expect a significantly reduced amount of exchangeable hydroxyl groups in the freeze-dried cellulose as compared with the native hydrogel. Whereas the cellulose H/D exchange in the shell is not significantly affected by the incorporation of PCW polysaccharides, the exchange within the core is reduced in the composite hydrogel containing xyloglucan. Such an effect may be related to the presence of a certain fraction

of this PCW polysaccharide strongly interacting with the cellulose microfibrils contained within the ribbons' core region, hence limiting the availability of the cellulose hydroxyl groups to be exchanged.

Table 3a. Parameters obtained from fits of the power-law plus core-shell cylinder with polydisperse radius model for the pure BC hydrogel. Standard deviations on the last digit are shown in parentheses.

	93%D_2O	56%D_2O	33%D_2O	18%D_2O	0% D_2O
Scale factor	0.0038 (2)	0.0011 (3)	0	0.0016 (8)	0.0300 (7)
Core radius (nm) (+)	11.2 (2)	11.2 (2)	11.2 (2)	11.2 (2)	11.2 (2)
Cylinder length (nm) (+)(*)	500	500	500	500	500
Polydispersity (+)(*)	0.2	0.2	0.2	0.2	0.2
Radial shell thickness (nm) (+)	5.6 (8)	5.6 (8)	5.6 (8)	5.6 (8)	5.6 (8)
Cellulose volume fraction (Core) (+)	0.228 (6)	0.228 (6)	0.228 (6)	0.228 (6)	0.228 (6)
Cellulose volume fraction (Shell) (+)	0.001 (2)	0.001 (2)	0.001 (2)	0.001 (2)	0.001 (2)
Cellulose exchange (core) (+)	0.70 (3)	0.70 (3)	0.70 (3)	0.70 (3)	0.70 (3)
Cellulose exchange (shell) (+)	1.0 (8)	1.0 (8)	1.0 (8)	1.0 (8)	1.0 (8)
Solvent exchange (core) (+)	0.576 (1)	0.576 (1)	0.576 (1)	0.576 (1)	0.576 (1)
Solvent exchange	1	1	1	1	1

(shell) (+)(*)					
SLD cellulose (10^{10} cm^{-2}) (+)(*)	1.87	1.87	1.87	1.87	1.87
SLD fully exchanged cellulose (10^{10} cm^{-2}) (*)	3.66	2.95	2.50	2.23	1.87
SLD bulk solvent (10^{10} cm^{-2}) (*)	5.89	3.33	1.73	0.69	-0.56
SLD bound solvent (10^{10} cm^{-2}) (*)	7.97	4.50	2.33	1.03	-0.70
SLD bound H_2O (10^{10} cm^{-2}) (+)(*)	-0.70	-0.70	-0.70	-0.70	-0.70
Power-law coefficient	$11.85 \cdot 10^{-5}$ (5)	$4.36 \cdot 10^{-5}$ (8)	$0.5 \cdot 10^{-5}$ (7)	$1.79 \cdot 10^{-5}$ (5)	$8.68 \cdot 10^{-5}$ (7)
Power-law exponent	2.709 (9)	2.477 (4)	2.47 (3)	2.499 (5)	2.536 (2)

Parameters displayed with (+) were linked and parameters displayed with (*) were fixed during the fitting process.

Table 3b. Parameters obtained from fits of the power-law plus core-shell cylinder with polydisperse radius model for BC-AX hydrogel. Standard deviations on the last digit are shown in parentheses.

	93%D_2O	56%D_2O	33%D_2O	18%D_2O	0% D_2O
Scale factor	0.0023 (1)	0.0010 (1)	0	0.0010 (1)	0.018 (1)
Core radius (nm) (+)	12.6 (2)	12.6 (2)	12.6 (2)	12.6 (2)	12.6 (2)
Cylinder length (nm) (+)(*)	500	500	500	500	500
Polydispersity (+)(*)	0.2	0.2	0.2	0.2	0.2

Radial shell thickness (nm) (+)	8.2 (3)	8.2 (3)	8.2 (3)	8.2 (3)	8.2 (3)
Cellulose volume fraction (Core) (+)	0.27 (1)	0.27 (1)	0.27 (1)	0.27 (1)	0.27 (1)
Cellulose volume fraction (Shell) (+)	0.011 (3)	0.011 (3)	0.011 (3)	0.011 (3)	0.011 (3)
Cellulose exchange (core) (+)	0.69 (4)	0.69 (4)	0.69 (4)	0.69 (4)	0.69 (4)
Cellulose exchange (shell) (+)	0.7 (7)	0.7 (7)	0.7 (7)	0.7 (7)	0.7 (7)
Solvent exchange (core) (+)	0.599 (2)	0.599 (2)	0.599 (2)	0.599 (2)	0.599 (2)
Solvent exchange (shell) (+)(*)	1	1	1	1	1
SLD cellulose (10^{10} cm^{-2}) (+)(*)	1.87	1.87	1.87	1.87	1.87
SLD fully exchanged cellulose (10^{10} cm^{-2}) (*)	3.66	2.95	2.50	2.23	1.87
SLD bulk solvent (10^{10} cm^{-2}) (*)	5.89	3.33	1.73	0.69	-0.56
SLD bound solvent (10^{10} cm^{-2}) (*)	7.97	4.50	2.33	1.03	-0.70
SLD bound H_2O (10^{10} cm^{-2}) (+)(*)	-0.70	-0.70	-0.70	-0.70	-0.70
Power-law coefficient	$16.53 \cdot 10^{-5}$ (5)	$4.69 \cdot 10^{-5}$ (6)	$0.6 \cdot 10^{-5}$ (3)	$3.98 \cdot 10^{-5}$ (6)	$12.31 \cdot 10^{-5}$ (8)
Power-law exponent	2.656 (1)	2.529 (3)	2.55 (1)	2.485 (5)	2.496 (2)

Parameters displayed with (+) were linked and parameters displayed with (*) were fixed during the fitting process.

Table 3c. Parameters obtained from fits of the power-law plus core-shell cylinder with polydisperse radius model for BC-XG hydrogel. Standard deviations on the last digit are shown in parentheses.

	93%D_2O	56%D_2O	33%D_2O	18%D_2O	0% D_2O
Scale factor	0.0043 (1)	0.0010 (1)	0	0.0010 (7)	0.022 (1)
Core radius (nm) (+)	14.1 (7)	14.1 (7)	14.1 (7)	14.1 (7)	14.1 (7)
Cylinder length (nm) (+)(*)	500	500	500	500	500
Polydispersity (+)(*)	0.2	0.2	0.2	0.2	0.2
Radial shell thickness (nm) (+)	6.8 (5)	6.8 (5)	6.8 (5)	6.8 (5)	6.8 (5)
Cellulose volume fraction (Core) (+)	0.213 (4)	0.213 (4)	0.213 (4)	0.213 (4)	0.213 (4)
Cellulose volume fraction (Shell) (+)	0.002 (2)	0.002 (2)	0.002 (2)	0.002 (2)	0.002 (2)
Cellulose exchange (core) (+)	0.33 (3)	0.33 (3)	0.33 (3)	0.33 (3)	0.33 (3)
Cellulose exchange (shell) (+)	1.0 (7)	1.0 (7)	1.0 (7)	1.0 (7)	1.0 (7)
Solvent exchange (core) (+)	0.685 (1)	0.685 (1)	0.685 (1)	0.685 (1)	0.685 (1)
Solvent exchange (shell) (+)(*)	1	1	1	1	1

SLD cellulose (10^{10} cm^{-2}) (+)(*)	1.87	1.87	1.87	1.87	1.87
SLD fully exchanged cellulose (10^{10} cm^{-2}) (*)	3.66	2.95	2.50	2.23	1.87
SLD bulk solvent (10^{10} cm^{-2}) (*)	5.89	3.33	1.73	0.69	-0.56
SLD bound solvent (10^{10} cm^{-2}) (*)	7.97	4.50	2.33	1.03	-0.70
SLD bound H_2O (10^{10} cm^{-2}) (+)(*)	-0.70	-0.70	-0.70	-0.70	-0.70
Power-law coefficient	$14.05 \cdot 10^{-5}$ (5)	$4.75 \cdot 10^{-5}$ (8)	$0.9 \cdot 10^{-5}$ (4)	$3.05 \cdot 10^{-5}$ (5)	$9.75 \cdot 10^{-5}$ (7)
Power-law exponent	2.685 (1)	2.427 (4)	2.46 (1)	2.536 (5)	2.552 (2)

Parameters displayed with (+) were linked and parameters displayed with (*) were fixed during the fitting process.

It should be noted that, as observed in Figures 4A, 4B and 4C, the obtained fits deviate from the experimental data within the high q region ($q > 0.10$ $Å^{-1}$). Considering the real distances corresponding to this q range (i.e. real distances smaller than ca. 6 nm), the inability of the model to accurately describe the experimental data may be related to the existence of sub-structure within the cellulose ribbons. While the core-shell model applied to fit the SANS data is derived from the assumption that a number of cellulose microfibrils, interacting with each other and with bound solvent by means of hydrogen bonding, compose the ribbon structure, the fitting function only accounts for the core-shell ribbon architecture. Thus, while the scattering in the high q region is likely to be dominated from the structural arrangement of cellulose microfibrils, the fitting function does not contain

any additional term to account for this particular size range. This would explain the discrepancy between the theoretical and the experimental points within the region of q > 0.10 $Å^{-1}$. As opposed to neutrons, X-rays are sensitive to electron density; as a result, measurement by SAXS is not expected to reveal the creation of regions arising from differential solvent accessibility within the ribbons' core and shell as cellulose in both regions are solvated with the same solvent. Instead, assuming the validity of the multi-scale architecture depicted in Figure 7, the X-ray SLD contrast would be generated between the crystalline and paracrystalline cellulose domains and therefore, the SAXS intensity should be dominated by the structural features arising from the arrangement of cellulose microfibrils. To assess the veracity of this, the SAXS patterns of the native cellulose and composite hydrogels were collected and the experimental data were fitted by using the core-shell model adapted to the microfibril structural level, as described in section 2.4. As shown in Figure 5, the microfibril core-shell model provides excellent fits for the experimental data, with reduced χ^2 values of 1.5, 1.9 and 1.5 for the BC, BC-AX and BC-XG hydrogels, respectively. The corresponding fitting parameters, compiled in Table S2, support the existence of microfibrils containing an impermeable crystalline interior region (i.e. microfibril core) surrounded by a partially hydrated paracrystalline exterior (i.e. microfibril shell). The overall microfibril dimensions, estimated from the core radius and shell thickness, are ca. 5.0 nm for the BC hydrogel, 4.5 nm for BC-AX and 3.6 nm for BC-XG. These values are very similar to the range of crystallite dimensions previously calculated for similar samples by means of XRD characterisation (5.2-5.9 nm for BC, 4.9-5.4 nm for BC-AX and 3.9-5.0 nm for BC-XG) [10], hence supporting the ability of the fitting function to model the structure of the individual cellulose microfibrils contained within the ribbons. Interestingly, while the cellulose volume fraction within the microfibril shell is ca. 60% for the BC and the BC-AX hydrogels, the fitting results

indicate that the BC-XG hydrogel possesses a reduced volume fraction of ca. 30%. Such an effect may be due to the presence of xyloglucan in the paracrystalline microfibril shell, supporting the hypothesis of strong cellulose-xyloglucan interactions being established at the microfibril structural level.

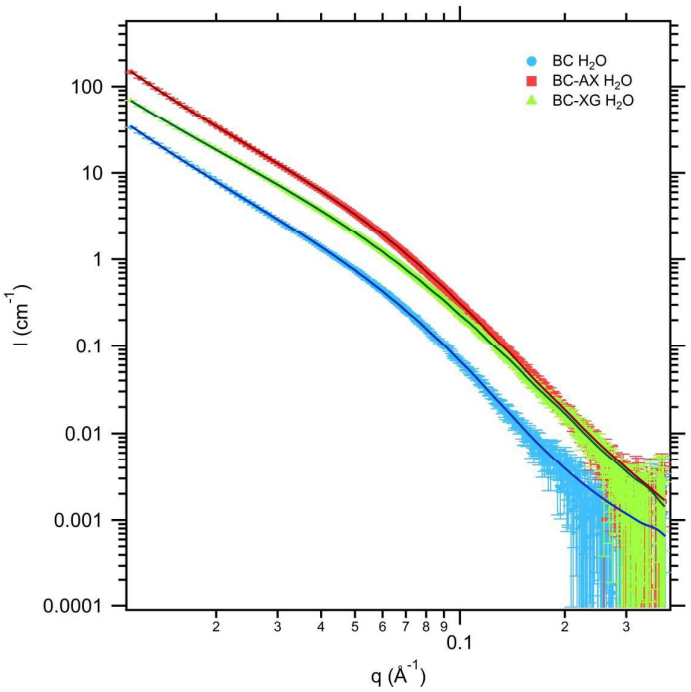

Figure 5. SAXS patterns for the native BC, BC-AX and BC-XG hydrogels. Solid lines correspond to the fitting of the experimental data using the core-shell model applied at the cellulose microfibril structural level.

The results from the SANS experiments, further supported by the SAXS characterisation, have two main implications: (i) the PCW polysaccharide surface domains promote solvent accessibility towards the interior of the cellulose ribbons; and (ii) the arabinoxylan and xyloglucan components interact with cellulose through different mechanisms. Whereas both PCW polysaccharides seem to interact with the cellulose ribbons' surface, only xyloglucan is able to establish strong interactions with the individual cellulose microfibrils composing the ribbons' core by interfering in the cellulose crystallization and assembly

processes. This is consistent with results from microscopy and ^{13}C-NMR spectroscopy of BC-AX and BC-XG composites [17, 29, 55, 56]. Whereas two distinct domains of xyloglucan were detected in the ^{13}C CP/MAS and SP/MAS spectra of BC-XG hydrogels (with approximately half of the xyloglucan corresponding to the mobile phase and the other half being effectively immobilised), arabinoxylan was only detected in the ^{13}C SP/MAS spectrum of BC-AX hydrogels [55, 56]. This observation supports the existence of different xyloglucan domains (mobile domains interacting with the surface of cellulose ribbons and strongly bound domains interspersed with individual cellulose microfibrils composing the ribbons), while only surface interactions appear to take place between arabinoxylan and cellulose. The presence of xyloglucan domains interacting with cellulose microfibrils has important implications for the biosynthesis process. It has been previously demonstrated that the interference of xyloglucan with the cellulose crystallisation process leads to the formation of smaller crystallites, richer in the I_β allomorph, which are similar to those typically found in PCW systems [10]. Additionally, it has been proposed that the tightly bound xyloglucan interfibrillar domains, rather than the mobile fractions tethering the cellulose bundles, play a major role in the cell wall mechanics [57]. In contrast, the mobile surface domains of both xyloglucan and arabinoxylan increase the degree of branching of the hydrogel network structure and increase the amount of labile hydroxyl groups at a surface level. This may play an important role in controlling the hydrophilicity of the surface of cellulose ribbons and thus is crucial for plant tissues.

It should be noted that, while the model here presented seems to be appropriate to describe the multi-scale structure of bacterial cellulose hydrogels, its ability to describe the small angle scattering data from PCW materials would need to be assessed for each particular system. One of the key aspects of the core-shell formalism lies in its ability to account for

the existence of regions with different SLD values, due to the distinct solvent accessibility towards the interior and exterior regions of the ribbons. While the existence of strong hydrogen bonds between cellulose microfibrils is a plausible assumption since no additional components are present during the cellulose biosynthesis process [10], this might not be the case for certain PCW systems, in which matrix components directly interacting with the cellulose microfibrils may limit the formation of interfibrillar hydrogen bonds. In fact, the shoulder features shown here for the bacterial cellulose hydrogels have not been observed in the SANS patterns of celery and spruce wood samples [4, 8]. In turn, an interference peak located at 0.1-0.2 $Å^{-1}$, attributed to the centre-to-centre distance between the cellulose microfibrils, was detected for these materials. The position of this peak shifted towards smaller q values when the samples were hydrated [4, 8], hence indicating that water could penetrate the bundles of microfibrils and increase the microfibril centre-to-centre distance. The contrast between the crystalline microfibril interior and the surrounding bulk solvent would then lead to the appearance of a Bragg peak characteristic of the interfibrillar separation, whereas no core-shell regions with distinct SLD values would be apparent in that particular case.

Solvent contrast variation experiments were also used to estimate the contrast match point of the three different materials. Following scattering measurements, the intensity at a q value of 0.0052 $Å^{-1}$ was plotted against the D_2O content of the solvent mixtures utilised (cf. Figure 6A). To evaluate the percentage error associated with the determination of the scattering intensity values, several bacterial cellulose samples soaked in H_2O were studied and the intensity at the same q value used for the contrast match point determination was measured (cf. Figure S2). These samples consisted of four different batches harvested under the same conditions but not simultaneously, taking two different sample portions

from each batch (thus making a total of eight samples). The maximum standard deviation determined for different samples from the same batch was ca. 6.2%, whereas the standard deviation determined from all eight samples was ca. 24.1%. This latter value was set as the intensity error percentage (error bars in Figure 6A). As observed in Figure 6A, the contrast match point of the three different materials, estimated by fitting the experimental data to a parabolic function and subsequently calculating the function minimum, was quite similar (ca. 34.2% D_2O for BC, ca. 34.9% D_2O for BC-AX and ca. 35.9% for BC-XG). Indeed, the resulting SLD of ca. $1.81 \cdot 10^{10}$ cm^{-2} for pure bacterial cellulose is very close to the crystalline cellulose theoretical value listed in Table 1. According to the crystallinity index of the bacterial cellulose hydrogels used in this work, which has been previously estimated as ca. 88% [10], a SLD value of $1.85 \cdot 10^{10}$ cm^{-2} would be expected. Although the contrast match point of cellulose samples has been typically estimated by neglecting the effect of H/D exchange, cellulose possesses labile hydroxyl groups which are in fact expected to undergo exchange when the samples are soaked in D_2O/H_2O mixtures. Thus the SLD of cellulose should increase with the amount of D_2O in the solvent for any finite degree of H/D exchange and, as a result, the experimentally obtained contrast variation curves deviate from the contrast variation curve observed in the absence of H/D exchange and consequently, the approach followed to determine the SLD by fitting the experimental points to a parabolic function would not provide an accurate value.

The H/D exchange process in cellulose samples has been reported to occur in two different stages. During the relatively short first stage, H/D exchange is thought to take place in the hydroxyl groups located within the cellulose amorphous domains [58, 59]. The duration of this process is related to the sample properties (such as sample thickness and cellulose crystallinity). As a reference, Hishikawa et al. stated that this process took place within

several hours, with a gradual transition towards the subsequent exchange stage [58]. Within the second stage, H/D exchange takes place at a significantly slower rate, ranging from several hours to days. This process has been related to the exchange of hydroxyl groups found in the cellulose crystallites' surfaces or regions with increased disorder (i.e. paracrystalline cellulose) [59]. Considering that the hydrogel samples used for the SANS contrast variation experiments were soaked in H_2O/D_2O mixtures for periods longer than 48h, the H/D exchange process in the hydroxyl groups located within accessible regions is expected to be complete. The degree of H/D exchange undergone by each hydrogel should be determined by the cellulose structure, i.e. the relative amount of accessible paracrystalline cellulose, as well as by the interactions established between the cellulose and the PCW polysaccharides in the composite hydrogels. To evaluate the extent of the H/D exchange effect, the shape of the theoretical contrast variation curves, assuming a certain degree of H/D exchange, was predicted by calculating the square of the SLD contrast between the bacterial cellulose hydrogel and the surrounding solvent since the intensity, $I \propto (SLD_{BC} - SLD_{solvent})^2$. The SLD of native bacterial cellulose, with the molecular formula of $C_6H_{10}O_5$, can be calculated as follows:

$$SLD_{BC}{}^{*} = N_A \cdot \rho_{BC} \cdot \frac{6b_C+5b_O+10b_H}{6M_C+5M_O+10M_H} \quad (8)$$

where b_i and M_i are the neutron scattering length and mass of the atoms, respectively and ρ_{BC}, i.e. the physical density of bacterial cellulose, would correspond to a value of 1.59 g/cm^3 according to the previously calculated crystallinity index of bacterial cellulose [10] and to the crystalline and amorphous cellulose density values provided in Table 1.

When the cellulose hydrogels are soaked in D_2O, a maximum of three hydrogen atoms, corresponding to the labile hydroxyl groups, can be exchanged; thus the molecular formula

of fully exchanged cellulose would be $C_6H_7D_3O_5$. Accordingly, for an intermediate degree of H/D exchange ($exc_{H/D}$) the SLD can be estimated as:

$$SLD_{BCexc}{}^{*} = N_A \cdot \rho_{BC} \cdot \frac{6b_C+5b_O+(10-(3\cdot exc_{H/D}))b_H+(3\cdot exc_{H/D})b_D}{6M_C+5M_O+\left(10-(3\cdot exc_{H/D})\right)M_H+(3\cdot exc_{H/D})M_D} \quad (9)$$

Hence, combining equations (8) and (9) and assuming a degree of H/D exchange with the solvent (which is in vast excess with respect to the polymer), the SLD of cellulose for each D_2O/H_2O mixture (where x_{D_2O} is the corresponding D_2O volume fraction) may be calculated by applying the following equation:

$$SLD_{BCexc} = x_{D_2O} \cdot SLD_{BCexc}{}^{*} + (1 - x_{D_2O}) \cdot SLD_{BC}{}^{*} \quad (10)$$

Figure 6B displays the term $(SLD_{BC} - SLD_{solvent})^2$ plotted against the D_2O volume fraction, considering different degrees of H/D exchange. As expected, the contrast match point is shifted towards greater D_2O volume fraction values with increasing the H/D exchange. The shape of the contrast variation curve of the bacterial cellulose hydrogel should then correspond to an intermediate of the different curves plotted in Figure 5B, i.e. as the D_2O volume fraction increases, the corresponding point would deviate from the 0% H/D exchange curve to a greater extent and would progressively become closer to the behaviour of the 100% H/D exchange curve. This is expected to affect significantly the shape of the experimental contrast variation curve, which will deviate from the theoretical parabolic function. Using the parameters obtained by application of the core-shell fitting model, listed in Table 3a, the SLD contrast terms for the ribbon core and shell were also estimated. As observed, for low D_2O volume fractions, the core and shell values are quite similar, whereas the difference between their corresponding SLD contrast terms increases with greater D_2O volume fractions. According to the ribbon model shown in Figure 7,

where the shell constitutes only a limited fraction of the ribbon, the experimental points should be closer to the values predicted for the ribbon core (i.e. 70% exchange).

Regarding the composite hydrogels, based on the incorporation degrees of the two polysaccharides estimated from the monosaccharide analysis, i.e. 53% AX and 27% XG, and the crystallinity values estimated by XRD [10] (ca. 87% for BC-AX and ca. 64% for BC-XG), the expected SLD values for the BC-AX and BC-XG samples would be $1.73 \cdot 10^{10}$ cm^{-2} and $1.77 \cdot 10^{10}$ cm^{-2}, respectively. However, the values estimated from the contrast variation experiments, $1.86 \cdot 10^{10}$ cm^{-2} for BC-AX and $1.93 \cdot 10^{10}$ cm^{-2} for BC-XG, although close, are slightly higher. The incorporation of PCW polysaccharides into the hydrogels might promote H/D exchange due to the addition of amorphous chains possessing labile hydroxyl groups; however, conversely, the interaction of these polysaccharides with cellulose chains by hydrogen bonding could limit the amount of free hydroxyl groups available for exchange. Thus, predicting the shape of the contrast variation curves for the composite hydrogels is more challenging since it requires assumptions concerning the degree of H/D exchange undergone by the AX and XG chains as well as the fraction of hydroxyl groups involved in strong hydrogen bonds established between cellulose and the polysaccharide chains which, at the same time, are expected to be different within the core and the shell regions. Attempts to estimate the theoretical contrast variation curves for the composite hydrogels confirmed that it is not possible to accurately quantify the effect of these two polysaccharides in the contrast match point of the composite hydrogels, as more information with regards to their structure and preferential location (i.e. ribbons' core and shell) would be required.

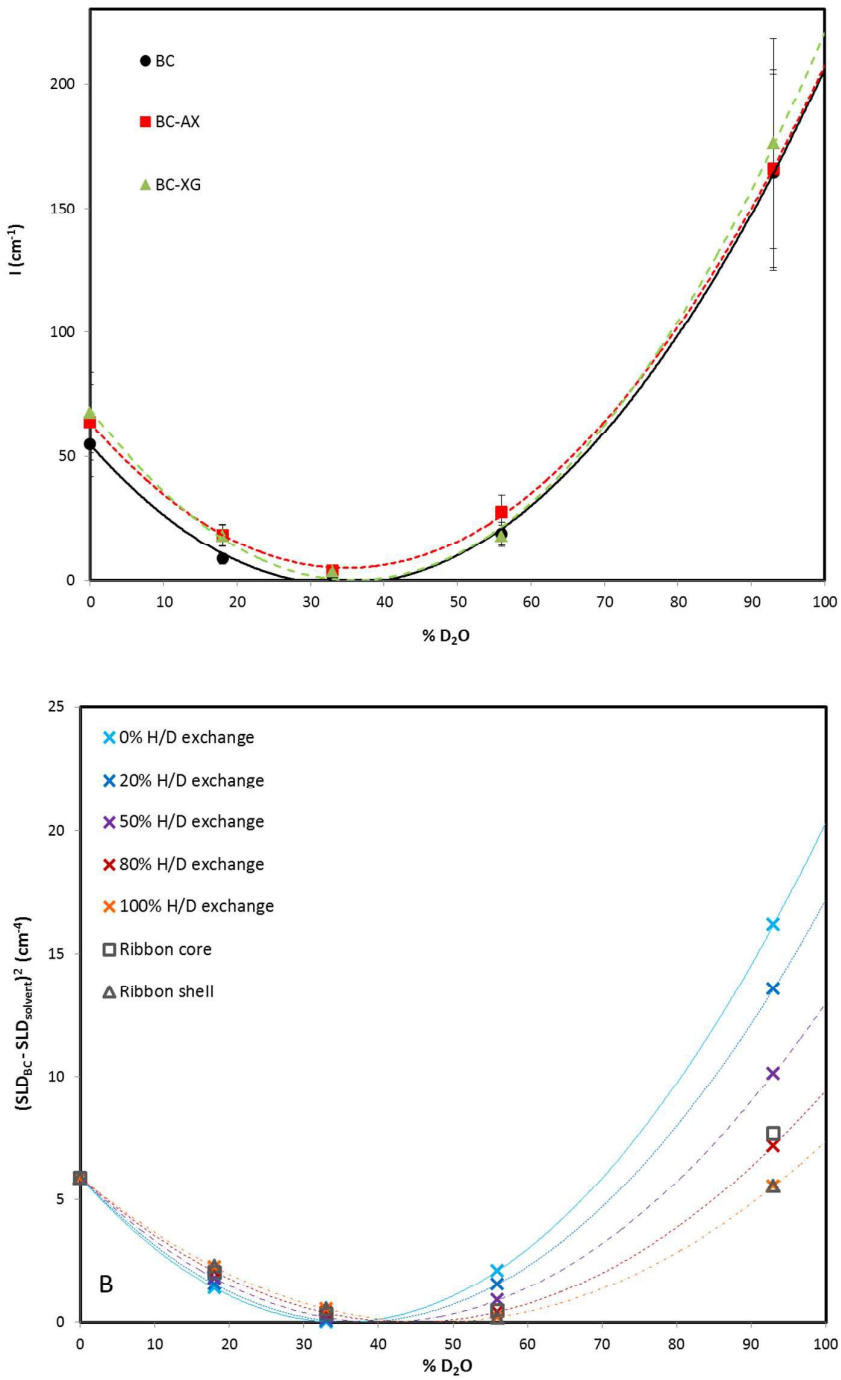

Figure 6. (A) Contrast variation curves for BC, BC-AX and BC-XG hydrogels. Markers represent the experimental values and the solid lines correspond to the fitted parabolic functions. (B) Representation of the SLD contrast term $(SLD_{BC}\text{-}SLD_{solvent})^2$ as a function of the D_2O content of the different solvent mixtures used for the contrast variation experiments of pure BC. Crosses represent the theoretical values calculated by assuming

different degrees of H/D exchange and solid lines correspond to the parabolic functions fitting the theoretical values. The values predicted by the fitting model for the ribbon core and shell, using the parameters summarised in Table 3a, are also displayed as open markers for comparison.

The results demonstrate that the developed SANS model of native bacterial cellulose and its composite hydrogels with PCW polysaccharides may provide valuable information to investigate the structure of these materials as well as the effect of different components on the hierarchical assembly of cellulose. It should be noted that the model assumes a cylindrical cellulose ribbon cross-section, which may be in conflict with the rectangular shape presumed in several studies according to TEM observations. However, it is relevant to consider that the drying process applied prior to the TEM characterisation inevitably impacts upon the structure of the cellulose ribbons, although it is still unknown how. Even if the flat ribbon cross-section was true, the periodic twisting along the ribbon axis also observed in the TEM images would lead to an overall morphology which could be approximated to a cylinder. As an additional comment, it is worth noting that although the model is built on the basis of the existence of sub-structure within the ribbons, it does not account for the structure of the individual cellulose microfibrils, leading to deviation from the experimental data within the relevant size range ($q > 0.10$ Å^{-1}). Including an additional term to describe the microfibril structure would result in an excessive number of refinable parameters and most likely lead to high uncertainties in the fitting results. However, it has been demonstrated that the same fitting function, adapted to account for the microfibril structural level, can be successfully applied to describe the SAXS results from the same hydrogels. This supports the existence of a multi-scale structure in which individual cellulose microfibrils, composed of an impermeable crystalline core and a partially

hydrated paracrystalline shell, interact with each other and with solvent by hydrogen bonding, creating the cellulose ribbons. Whereas the use of X-rays highlights the microfibril structure due to the SLD contrast existing between the crystalline and the paracrystalline regions, the structure of ribbons is emphasised when using neutrons. The strong hydrogen bonding network holding together the cellulose microfibrils impairs the solvent accessibility towards the inner region of the cellulose ribbons. This leads to the creation of core and shell regions with different neutron SLD values due to their different degrees of solvent exchange.

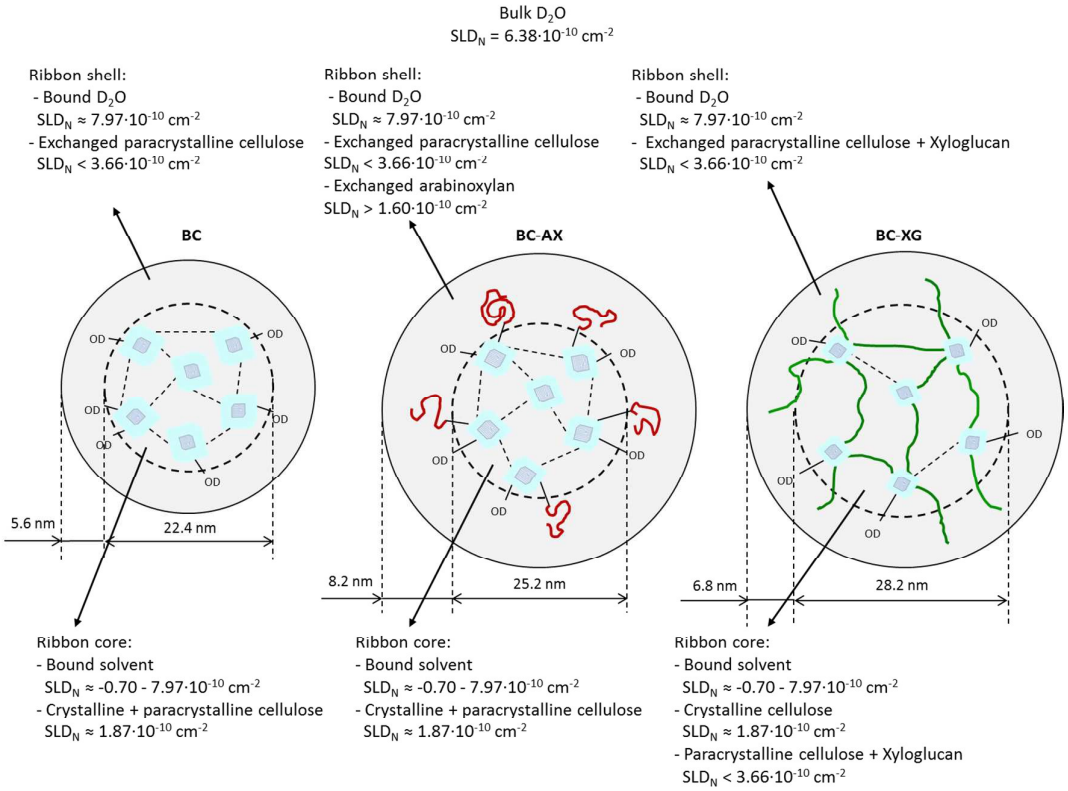

Figure 7. Schematic representation of the structure of hydrated (D_2O soaked) bacterial cellulose and composite ribbons based on fitting parameters obtained by the power-law plus core-shell cylinder with polydisperse radius model applied to SANS experimental data. Representation of the sub-structure of microfibrils is based on the parameters

obtained by fitting the SAXS data of the native hydrogels and the cellulose crystallite cross-sectional shape suggested in previous work [10] from XRD experiments.

4. Conclusions

Structural characterisation of native bacterial cellulose and its composite hydrogels with two PCW polysaccharides has been carried out by means of small angle neutron scattering and a model has been developed that well describes the experimental data over a wide intensity - q range. It has been demonstrated that application of conventional models proposed in the existing literature, such as a parallelepiped or large disk model, do not provide adequate fits of the SANS data. This is due to the fact that these models consider bacterial cellulose ribbons as one-phase solid objects with uniform SLD.

In contrast, the hierarchical assembly of bacterial cellulose, in which structural features are assembled into several architectural levels, may be well represented by a core-shell formalism; this assumes that the ribbons are composed of an inner region (core) mostly containing impermeable cellulose crystallites surrounded by a network of hydrated paracrystalline cellulose and tightly bound water, and an outer region (shell) containing highly hydrated paracrystalline cellulose and water. The different core and shell solvent accessibilities implied by this arrangement result in the formation of regions with distinct neutron SLD values when the hydrogels are soaked in H_2O/D_2O mixtures. Based on this, a model comprising the sum of a power-law term plus a core-shell cylinder with polydisperse radius was developed and validated by fitting the SANS contrast variation data of pure and composite bacterial cellulose samples. The developed model has been demonstrated to provide acceptable fits over greater than three orders of magnitude in q

not only with a limited number of variable parameters but also whose refined values are physically sensible and meaningful based on prior knowledge of the systems under study.

The obtained fitting parameters indicate that both xyloglucan and arabinoxylan domains exist on the surface of bacterial cellulose ribbons interacting with the cellulose fraction by means of a non-specific adsorption mechanism, therefore providing additional hydroxyl groups in the ribbons' shell and facilitating the access of the solvent towards the ribbons' core. On the other hand, the fitting results, together with a careful analysis of the contrast variation curves, seem to indicate that, only xyloglucan seems to establish strong interactions with the cellulose microfibrils contained within the ribbons' core by interacting with the crystallisation/assembly process. The existence of these xyloglucan domains within the core region is crucial as it has been seen to modify the cellulose crystalline structure (decreasing the overall crystallinity and promoting the creation of the plant-characteristic I_β allomorph) and the packing density by separating the individual cellulose microfibrils. This supports a different cellulose/xyloglucan [19] and cellulose/arabinoxylan [29] interaction mechanism and, furthermore, highlights the potential of this approach to characterise additional PCW analogue systems based on bacterial cellulose, hence providing valuable information to interpret the potential roles of different cell wall components on the biosynthesis process.

Acknowledgements

MMS would like to acknowledge a postdoctoral fellowship jointly funded by ANSTO and the ARC Centre of Excellence in Plant Cell Walls. Drs. Patricia Lopez-Sanchez and Dongjie Wang are acknowledged for the production of pure bacterial cellulose hydrogels and its composites.

References

1. D. P. Delmer and Y. Amor, *Plant Cell*, 1995, **7**, 987-1000.

2. M. Mutwil, S. Debolt and S. Persson, *Current Opinion in Plant Biology*, 2008, **11**, 252-257.

3. O. M. Astley and A. M. Donald, *Biomacromolecules*, 2001, **2**, 672-680.

4. A. N. Fernandes, L. H. Thomas, C. M. Altaner, P. Callow, V. T. Forsyth, D. C. Apperley, C. J. Kennedy and M. C. Jarvis, *Proceedings of the National Academy of Sciences of the United States of America*, 2011, **108**, E1195-E1203.

5. M. A. Ha, D. C. Apperley, B. W. Evans, M. Huxham, W. G. Jardine, R. J. Vietor, D. Reis, B. Vian and M. C. Jarvis, *Plant Journal*, 1998, **16**, 183-190.

6. C. J. Kennedy, G. J. Cameron, A. Sturcova, D. C. Apperley, C. Altaner, T. J. Wess and M. C. Jarvis, *Cellulose*, 2007, **14**, 235-246.

7. R. H. Newman, S. J. Hill and P. J. Harris, *Plant Physiology*, 2013, **163**, 1558-1567.

8. L. H. Thomas, V. Trevor Forsyth, A. Šturcová, C. J. Kennedy, R. P. May, C. M. Altaner, D. C. Apperley, T. J. Wess and M. C. Jarvis, *Plant Physiology*, 2013, **161**, 465-476.

9. C. Castro, R. Zuluaga, J. L. Putaux, G. Caro, I. Mondragon and P. Gañán, *Carbohydrate Polymers*, 2011, **84**, 96-102.

10. M. Martínez-Sanz, P. Lopez-Sanchez, M. J. Gidley and E. P. Gilbert, *Cellulose*, 2015, **22**, 1541-1563.

11. R. T. Olsson, R. Kraemer, A. Lopez-Rubio, S. Torres-Giner, M. J. Ocio and J. M. Lagaron, *Macromolecules*, 2010, **43**, 4201-4209.

12. T. Fujino and T. Itoh, *Protoplasma*, 1994, **180**, 39-48.

13. J. Sugiyama, H. Harada, Y. Fujiyoshi and N. Uyeda, *Planta*, 1985, **166**, 161-168.

14. T. I. Baskin, in *Annu. Rev. Cell Dev. Biol.*, 2005, vol. 21, pp. 203-222.

15. A. Geitmann, *Current Opinion in Plant Biology*, 2010, **13**, 693-699.

16. A. Reiterer, H. Lichtenegger, S. Tschegg and P. Fratzl, *Philosophical Magazine a-Physics of Condensed Matter Structure Defects and Mechanical Properties*, 1999, **79**, 2173-2184.

17. M. Martínez-Sanz, M. J. Gidley and E. P. Gilbert, *Carbohydrate Polymers*, 2015

,**125**, 120-134.

18. M. Iguchi, S. Yamanaka and A. Budhiono, *Journal of Materials Science*, 2000, **35**, 261-270.

19. R. M. Brown Jr, *Journal of Macromolecular Science - Pure and Applied Chemistry*, 1996, **33**, 1345-1373.

20. A. Endler and S. Persson, *Molecular Plant*, 2011, **4**, 199-211.

21. C. Tokoh, K. Takabe, J. Sugiyama and M. Fujita, *Cellulose*, 2002, **9**, 65-74.

22. A. R. White and R. M. Brown Jr, *Proceedings of the National Academy of Sciences of the United States of America*, 1981, **78**, 1047-1051.

23. C. Tokoh, K. Takabe, M. Fujita and H. Saiki, *Cellulose*, 1998, **5**, 249-261.

24. E. Chanliaud and M. J. Gidley, *Plant Journal*, 1999, **20**, 25-35.

25. J. Gu and J. M. Catchmark, *Cellulose*, 2013, **20**, 1613-1627.

26. D. Mikkelsen, M. J. Gidley and B. A. Williams, *Journal of Agricultural and Food Chemistry*, 2011, **59**, 4025-4032.

27. K. I. Uhlin, R. H. Atalla and N. S. Thompson, *Cellulose*, 1995, **2**, 129-144.

28. S. E. C. Whitney, J. E. Brigham, A. H. Darke, J. S. G. Reid and M. J. Gidley, *Carbohydrate Research*, 1998, **307**, 299-309.

29. S. E. C. Whitney, E. Wilson, J. Webster, A. Bacic, J. S. G. Reid and M. J. Gidley, *American Journal of Botany*, 2006, **93**, 1402-1414.

30. H. Yamamoto and F. Horii, *Cellulose*, 1994, **1**, 57-66.

31. H. Yamamoto, F. Horii and A. Hirai, *Cellulose*, 1996, **3**, 229-242.

32. A. Hirai, M. Tsuji, H. Yamamoto and F. Horii, *Cellulose*, 1998, **5**, 201-213.

33. O. M. Astley, E. Chanliaud, A. M. Donald and M. J. Gidley, *International Journal of Biological Macromolecules*, 2001, **29**, 193-202.

34. O. M. Astley, E. Chanliaud, A. M. Donald and M. J. Gidley, *International Journal of Biological Macromolecules*, 2003, **32**, 28-35.

35. J. He, S. V. Pingali, S. P. S. Chundawat, A. Pack, A. D. Jones, P. Langan, B. H. Davison, V. Urban, B. Evans and H. O'Neill, *Cellulose*, 2014, **21**, 927-936.

36. M. Khandelwal and A. H. Windle, *International Journal of Biological Macromolecules*, 2014, **68**, 215-217.

37. S. Koizumi, Z. Yue, Y. Tomita, T. Kondo, H. Iwase, D. Yamaguchi and T. Hashimoto, *European Physical Journal E*, 2008, **26**, 137-142.

38. P. C. S. F. Tischer, M. R. Sierakowski, H. Westfahl and C. A. Tischer, *Biomacromolecules*, 2010, **11**, 1217-1224.

39. D. Mikkelsen, B. M. Flanagan, S. M. Wilson, A. Bacic and M. J. Gidley, *Biomacromolecules*, 2015, 2015, **16**, 1232-1239.

40. D. Mikkelsen and M. J. Gidley, *Methods in molecular biology (Clifton, N.J.)*, 2011, **715**, 197-208.

41. E. P. Gilbert, J. C. Schulz and T. J. Noakes, *Physica B: Condensed Matter*, 2006, **385-386**, 1180-1182.

42. S. R. Kline, *Journal of Applied Crystallography*, 2006, **39**, 895-900.

43. A. P. Heiner and O. Teleman, *Langmuir*, 1997, **13**, 511-518.

44. J. F. Matthews, C. E. Skopec, P. E. Mason, P. Zuccato, R. W. Torget, J. Sugiyama, M. E. Himmel and J. W. Brady, *Carbohydrate Research*, 2006, **341**, 138-152.

45. M. Martínez-Sanz, A. Lopez-Rubio and J. Lagaron, *Carbohydrate Polymers*, 2011, **85**, 228-236.

46. M. Ioelovich, A. Leykin and O. Figovsky, *BioResources*, 2010, **5**, 1393-1407.

47. W. Chen, G. C. Lickfield and C. Q. Yang, *Polymer*, 2004, **45**, 1063-1071.

48. C. V. Cerclier, A. Guyomard-Lack, F. Cousin, B. Jean, E. Bonnin, B. Cathala and C. Moreau, *Biomacromolecules*, 2013, **14**, 3599-3609.

49. K. Zhang, *Applied Microbiology and Biotechnology*, 2013, **97**, 4353-4359.

50. H. P. Fink, H. J. Purz, A. Bohn and J. Kunze, *Macromolecular Symposia*, 1997, **120**, 207-217.

51. P. Lopez-Sanchez, M. Rincon, D. Wang, S. Brulhart, J. R. Stokes and M. J. Gidley, *Biomacromolecules*, 2014, **15**, 2274-2284.

52. P. Langan, L. Petridis, H. M. O'Neill, S. V. Pingali, M. Foston, Y. Nishiyama, R. Schulz, B. Lindner, B. Leif Hanson, S. Harton, W. T. Heller, V. Urban, B. R. Evans, S. Gnanakaran, A. J. Ragauskas, J. C. Smith and B. H. Davison, *Green Chemistry*, 2014, **16**, 63-68.

53. K.-Y. Lee, F. Quero, J. Blaker, C. S. Hill, S. Eichhorn and A. Bismarck, *Cellulose*, 2011, **18**, 595-605.

54. L. Fang and J. Catchmark, *Cellulose*, 2014, **21**, 3951-3963.

55. P. Lopez-Sanchez, J. Cersosimo, D. Wang, B. Flanagan, J. R. Stokes and M. J. Gidley, *PLoS ONE*, 2015, **10**, e0122132.

56. P. Lopez-Sanchez, E. Schuster, D. Wang, M. J. Gidley and A. Strom, *Soft Matter*, 2015, **11**, 4002-4010.

57. T. Wang, Y. B. Park, M. A. Caporini, M. Rosay, L. Zhong, D. J. Cosgrove and M. Hong, *Proceedings of the National Academy of Sciences*, 2013, **110**, 16444-16449.

58. Y. Hishikawa, E. Togawa, Y. Kataoka and T. Kondo, *Polymer*, 1999, **40**, 7117-7124.

59. K. Hofstetter, B. Hinterstoisser and L. Salmén, *Cellulose*, 2006, **13**, 131-145.